Research Article | Vol. 7, No. 8 | 1 Aug 2017 | OPTICAL MATERIALS EXPRESS 2871
Optical Materials EXPRESS

Study of plasmonics induced optical absorption enhancement of Au embedded in titanium dioxide nanohole arrays

YING ZHAO,[1] NILS HOIVIK,[1,2] MUHAMMAD NADEEM AKRAM,[1] AND KAIYING WANG[1,*]

[1]*Department of Micro and Nano Systems Technology, University College of Southeast Norway, Horten, 3184, Norway*
[2]*EnergyNest AS, 1396 Billingstad, Norway*
**Kaiying.Wang@usn.no*

Abstract: The light absorbing performance of titanium dioxide (TiO_2) nanohole arrays partially filled with metallic gold is investigated using analytical methods. As a plasmonic generation element on one-dimensional (1D) TiO_2, the shape and distribution of Au nanoparticles can be microfabricated controllably in 1D TiO_2 nanohole arrays rather than randomly loaded on their top surface. Results indicate that strong absorption enhancement and a large reception angle in the visible light region (λ = 700 - 850 nm) are induced due to the waveguide coupling within the nanohole arrays and surface plasmonic resonance (SPR) at the interface between TiO_2 and gold fillings. By varying the thickness of TiO_2 array or gold disks and the periodicity of nanohole array, a significant difference in plasmonic resonance wavelength and light absorption enhancement can be expected. Due to the symmetric configuration of the nanohole structure, the enhancement is insensitive to the polarization of the incoming light and the same enhancement factor can be achieved for both transverse electric (TE) and transverse magnetic (TM) modes. This model offers an approach to precisely control a 1D nanomaterial based plasmonic effect and can be adapted to other materials used in microelectromechanical systems industry.

OCIS codes: (160.5293) Photonic bandgap materials; (250.5403) Plasmonics; (220.4241) Nanostructure fabrication.

References and links

1. M. Grätzel, "Photoelectrochemical cells," Nature **414**(6861), 338–344 (2001).
2. B. O'Regan and M. Grätzel, "A low-cost, high-efficiency solar cell based on dye-sensitized," Nature **353**(6346), 737–740 (1991).
3. A. Fujishima and K. Honda, "Electrochemical photolysis of water at a semiconductor electrode," Nature **238**(5358), 37–38 (1972).
4. Y. Zhao, N. Hoivik, and K. Wang, "Recent advance on engineering titanium dioxide nanotubes for photochemical and photoelectrochemical water splitting," Nano Energy **30**, 728–744 (2016).
5. M. Wang, J. Ioccozia, L. Sun, C. Lin, and Z. Lin, "Inorganic-modified semiconductor TiO 2 nanotube arrays for photocatalysis," Energy Environ. Sci. **7**(7), 2182–2202 (2014).
6. G. K. Mor, O. K. Varghese, R. H. T. Wilke, S. Sharma, K. Shankar, T. J. Latempa, K. S. Choi, and C. A. Grimes, "P-type Cu-Ti-O nanotube arrays and their use in self-biased heterojunction photoelectrochemical diodes for hydrogen generation," Nano Lett. **8**(7), 1906–1911 (2008).
7. P. Roy, C. Das, K. Lee, R. Hahn, T. Ruff, M. Moll, and P. Schmuki, "Oxide nanotubes on Ti-Ru alloys: strongly enhanced and stable photoelectrochemical activity for water splitting," J. Am. Chem. Soc. **133**(15), 5629–5631 (2011).
8. N. K. Allam, A. J. Poncheri, and M. A. El-Sayed, "Vertically oriented Ti-Pd mixed oxynitride nanotube arrays for enhanced photoelectrochemical water splitting," ACS Nano **5**(6), 5056–5066 (2011).
9. Z. Liu, W. Hou, P. Pavaskar, M. Aykol, and S. B. Cronin, "Plasmon resonant enhancement of photocatalytic water splitting under visible illumination," Nano Lett. **11**(3), 1111–1116 (2011).
10. W. Wang, S. Wu, K. Reinhardt, Y. Lu, and S. Chen, "Broadband light absorption enhancement in thin-film silicon solar cells," Nano Lett. **10**(6), 2012–2018 (2010).
11. H. A. Atwater and A. Polman, "Plasmonics for improved photovoltaic devices," Nat. Mater. **9**(3), 205–213 (2010).
12. S. A. Maier, *Plasmonics: Fundamentals and Applications* (Springer Science & Business Media, 2007).

#291417 https://doi.org/10.1364/OME.7.002871
Journal © 2017 Received 27 Mar 2017; revised 21 Jun 2017; accepted 7 Jul 2017; published 12 Jul 2017

Optical Materials EXPRESS

13. R. A. Pala, J. White, E. Barnard, J. Liu, and M. L. Brongersma, "Design of plasmonic thin film solar cells with broadband absorption enhancements," Adv. Mater. **21**(34), 3504–3509 (2009).
14. C. Rockstuhl, S. Fahr, and F. Lederer, "Absorption enhancement in solar cells by localized plasmon polaritons," J. Appl. Phys. **104**(12), 123102 (2008).
15. C. G. Silva, R. Juárez, T. Marino, R. Molinari, and H. García, "Influence of excitation wavelength (UV or visible light) on the photocatalytic activity of titania containing gold nanoparticles for the generation of hydrogen or oxygen from water," J. Am. Chem. Soc. **133**(3), 595–602 (2011).
16. Z. Zhang, L. Zhang, M. N. Hedhili, H. Zhang, and P. Wang, "Plasmonic gold nanocrystals coupled with photonic crystal seamlessly on TiO2 nanotube photoelectrodes for efficient visible light photoelectrochemical water splitting," Nano Lett. **13**(1), 14–20 (2013).
17. M. Madou, *Fundamentals of Microfabrication and Nanotechnology*, Third Edition (CRC 2011).
18. S. E. Han and G. Chen, "Optical absorption enhancement in silicon nanohole arrays for solar photovoltaics," Nano Lett. **10**(3), 1012–1015 (2010).
19. B. Wang, T. Gao, and P. W. Leu, "Broadband light absorption enhancement in ultrathin film crystalline silicon solar cells with high index of refraction nanosphere arrays," Nano Energy **19**, 471–475 (2016).
20. L. Hu and G. Chen, "Analysis of optical absorption in silicon nanowire arrays for photovoltaic applications," Nano Lett. **7**(11), 3249–3252 (2007).
21. R. Wagner and W. Ellis, "Vapor-liquid-solid mechanism of single crystal growth," Appl. Phys. Lett. **4**(5), 89–90 (1964).
22. M. D. Kelzenberg, S. W. Boettcher, J. A. Petykiewicz, D. B. Turner-Evans, M. C. Putnam, E. L. Warren, J. M. Spurgeon, R. M. Briggs, N. S. Lewis, and H. A. Atwater, "Enhanced absorption and carrier collection in Si wire arrays for photovoltaic applications," Nat. Mater. **9**(3), 239–244 (2010).
23. K. Wang, G. Liu, N. Hoivik, E. Johannessen, and H. Jakobsen, "Electrochemical engineering of hollow nanoarchitectures: pulse/step anodization (Si, Al, Ti) and their applications," Chem. Soc. Rev. **43**(5), 1476–1500 (2014).
24. G. L. Chiarello, A. Zuliani, D. Ceresoli, R. Martinazzo, and E. Selli, "Exploiting the photonic crystal properties of TiO_2 nanotube arrays to enhance photocatalytic hydrogen production," ACS Catal. **6**(2), 1345–1353 (2016).
25. J.W. Marvin and J. Weber, *Handbook of Optical Materials* (CRC 2003).
26. E.D. Palik, *Handbook of Optical Constants of Solids* (Academic 1998).
27. S. Linic, P. Christopher, and D. B. Ingram, "Plasmonic-metal nanostructures for efficient conversion of solar to chemical energy," Nat. Mater. **10**(12), 911–921 (2011).
28. S. Eustis and M. A. el-Sayed, "Why gold nanoparticles are more precious than pretty gold: noble metal surface plasmon resonance and its enhancement of the radiative and nonradiative properties of nanocrystals of different shapes," Chem. Soc. Rev. **35**(3), 209–217 (2006).

1. Introduction

Due to abundant availability, low cost and anti-photo-corrosion properties, titanium dioxide (TiO_2) is considered to be a potential substitute for monocrystalline silicon for photo-voltaic applications [1, 2] and a promising candidate for other photochemical applications such as water splitting [3, 4] and biodegradation [5]. Yet, relatively low solar utilization percentage of TiO_2 material remains a challenge due to its large band gap (3.2 eV for anatase and 3.0 eV for rutile). Researches have shown that introduction of defects or dopants into the TiO_2 lattice can extend the absorption spectrum of TiO_2 into visible light region [6–9].

Surface plasmonic resonance (SPR) happens on certain structured metallic materials when the frequency of incoming photons matches the natural frequency of electron oscillation within the metal [4]. Nanograting is one of the classic structures which have been widely applied to silicon-based solar cells and photovoltaic devices to increase photon absorption efficiency and reduce the required thickness of Si thin film [10, 11]. With properly chosen periodicity and filling material in the grating slits, the SPR wavelength can be modified based on Eq. (1) [12]

$$\frac{2\pi}{P} = \frac{2\pi}{\lambda}\left(\frac{\varepsilon_1\varepsilon_2}{\varepsilon_1+\varepsilon_2}\right)^{\frac{1}{2}} \tag{1}$$

where ε_1 and ε_2 are dielectric constants of the metal and slit filling material, λ is the resonance wavelength and P is the periodicity of the grating structure. A conventional way to utilize a nanograting structure is to locate it on top of the functioning semiconductor materials [13, 14]. However, such approach results in blocking certain portion of incident solar photons. By

Optical Materials EXPRESS

placing nanogratings at the bottom of the optically active layer, the associated light-blocking issue can be largely avoided [10]. Yet, commonly used nanograting structures are polarization-dependent (sensitive to TM mode) and additional filling material is always required in order for SPR to occur within the desired visible or infrared light region. In the context of one dimensional TiO_2 nanostructures (1D TiO_2), one of the most commonly studied metallic structures for SPR generation is gold nanoparticle [9,15,16]. Experiments have shown that owing to the difference in shape and size of nanoparticles, different fractions of incoming light can be scattered into the substrate [11]. However, direct placement of particles on 1D TiO_2 either by physical evaporation [9] or by chemical synthesis [15, 16] results in randomly arranged clusters on top of the functioning material, which is not desirable for a MEMS/NEMS fabrication process where precise control of the structure is required [17].

In the last decade, a large amount of innovative and groundbreaking analytical work has enhanced the understanding of light absorption enhancement on silicon based solar cells and photovoltaic devices [10, 13, 18, 19], all of which have contributed to practical design and optimization [20]. However, there are very few studies focusing on TiO_2 who has great potential for creating new photovoltaic and photocatalytic devices in the future. According to Eq. (1), TiO_2 (relative permittivity ε = 6-8 in visible light region) itself can be the perfect filling material for Au grating slits with resonance wavelength of 650 - 850 nm corresponding to periodicity ranging from ~150 nm to ~350 nm.

In this study, square patterned TiO_2 nanohole arrays inspired by the work of Han et al. [18] are modeled with holes partially filled by thin Au nano-disks at the bottom. Such a structure can be implemented by following a series of typical microfabrication procedures as shown in Fig. 1 [17]. The square-arrayed silicon nanorod can be achieved via vapour-liquid-solid process described in [21, 22], and the structure is replicated by Poly(methyl methacrylate) (PMMA). TiO_2 nanohole arrays can then be formed by successive deposition and polish. After depositing gold back contact, the gold disks can be introduced to the hollow structure by electroplating as is suggested by Wang et al. [23]. Embedded at the bottom of nanoholes, the gold disks are confined within the nanohole arrays. Thus the periodicity and shape of gold fillings can be controlled via changing the dimensions of nanohole arrays. This proposed structure involves no alternate filling materials or blocking issue. Moreover, with hole arrays patterned in n (n≥2) dimensional symmetry perpendicular to the light illumination direction, the whole structure is expected to show rather low dependence on polarization direction.

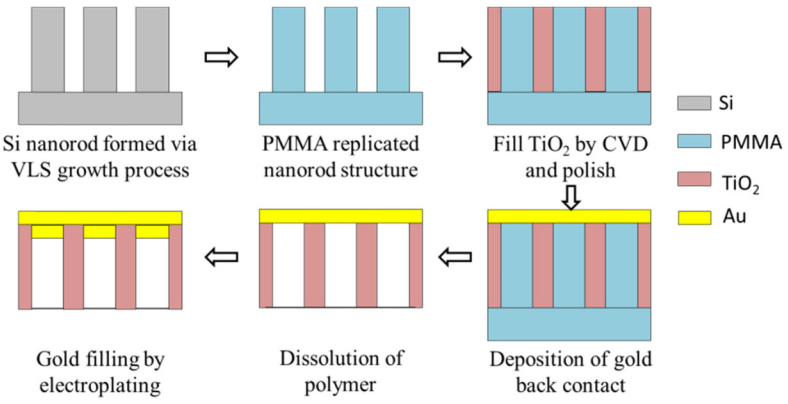

Fig. 1. Schematic view of the structure-implementation process. Different materials are indicated by colors.

Optical Materials EXPRESS

2. Model details

Figure 2 shows the scheme of the proposed square arranged of nanohole structure. The red-highlighted cell is a single unit cell we used during the simulation. Lines between unit cells are for illustration only. As indicated earlier, P is the periodicity of the array, t and d are the thickness and diameter of the filling gold layer, respectively, h is the depth of the holes (H = h-t) and T is the thickness of the gold back contact which is fixed at 50 nm. Making an analogy to electrochemically anodized nanotubes (Fig. 2), the d is inner diameter of the tube which is around P-30 nm (30 nm is the double of wall thickness). In addition, an air domain of 100 nm (not shown) is also defined on top of the cell.

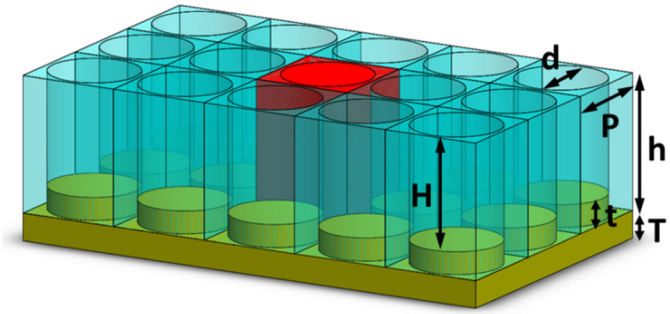

Fig. 2. Scheme of the proposed plasmon-enhanced nanohole structure and dimension notations.

As reported in [9, 24], light absorption beyond band gap of TiO_2 material is possible on 1D TiO_2 nanostructures considering photonic crystal properties and introduction of defects. We thus implemented simulation in the wavelength (λ) range that covers the whole visible light region: from 300 nm to 950 nm. Dispersive refractive indices of TiO_2 and Au were adopted from [25, 26]. For side and bottom boundaries of the unit cell, periodic condition and perfectly matching layers (PML) were applied, respectively. The absorption in the TiO_2 layer for a normally incident plane wave were calculated by Eq. (2) [13]

$$\omega \cdot \mathrm{Im}(\varepsilon) \int_V |E|^2 dV \tag{2}$$

where E is the local electric field and V is the volume of the TiO_2 nanostructure. Since the imaginary part of refractive index (Im(ε)) is largely dependent on periodicity and defects of 1D TiO_2 nanostructure, absolute value of the absorption calculated from adopted ε values cannot reveal the real case of our nanohole structure. Therefore the absorption enhancement factor (AEF) is introduced and defined as the ratio of absorption in the TiO_2 layer with and without Au disk fillings. According to Han et al. [18], absorbance of the nanohole arrays is dependent on filling fraction: the smaller the filling fraction is, the higher the absorbance becomes. We thus chose to employ a periodicity, which is related to filling fraction, of greater than 200 nm.

3. Results and discussion

Follow the parameters used by Wang *et al.* [10], our simulation was initiated with normal electromagnetic (EM) wave incidence using h = 150 nm, t = 50 nm. By sweeping parameters P within 240 - 360 nm and λ within 300 - 950 nm, we found no particular waveguide mode or SPR is excited under wavelength of 400 nm. Coupling into TiO_2 waveguide mode occurs when λ increases to around 400 nm and the strongest coupling is reached at λ = 650 nm for all P values without gold fillings. It is worth noting that the coupling is due to the patterned nanohole array structure and is affected only by the dimensions of the array (i.e. P and H). There is no sign of distinct coupling mode caused by adding gold into the holes. However,

Optical Materials EXPRESS

due to the addition of gold layer, H is reduced, which leads to a different coupling factor. For H = 100 nm, the strongest coupling shifts to λ = 600 nm. Figure 3 shows the local electric field distribution within TiO_2 material under TE mode (E in y direction) without (a) and with (b) gold filling at λ = 750 nm (where maximum electric field E_{max} is achieved). It is obvious that the electric field within TiO_2 is strengthened by more than one order of magnitude after introducing gold disk. Mapping of AEF with respect to incident wavelength and periodicity is shown in Fig. 3(c). Due to SPR effect, a maximum AEF of 7 can be observed at λ = 750 nm. It can be observed that the resonant frequency is red shifted from 700 nm to 800 nm as the periodicity increases from 240 nm to 360 nm, which agrees well to earlier results [10]. Compared to experimental results where gold nanoparticles are randomly distributed on TiO_2 nanostructures (SPR = 500 - 600 nm) [9, 15, 16], the proposed structure gives a red-shifted SPR (> 700 nm). This can be explained by the larger lateral dimension of Au compared to the gold particles/clusters formed in the experiments [27]. Additionally, absorption is found to be decreased at around λ = 400 nm and λ = 650 nm. AEF along the white dashed lines in Fig. 3(c) is displayed in Fig. 3(d) at different periodicity. The decrease feature at λ = 400 nm is independent of periodicity, which may be attributed to light absorption on gold nanostructure of low aspect ratio [28]. On the contrary, the decrease in AEF at around λ = 650 nm occurs only for certain P values, which can be explained by the aforementioned dependence of coupling modes on nanohole dimensions. Simulation results have proved that changing in both periodicity and vertical dimension of holes can lead to different coupling of E-field in the entire structure.

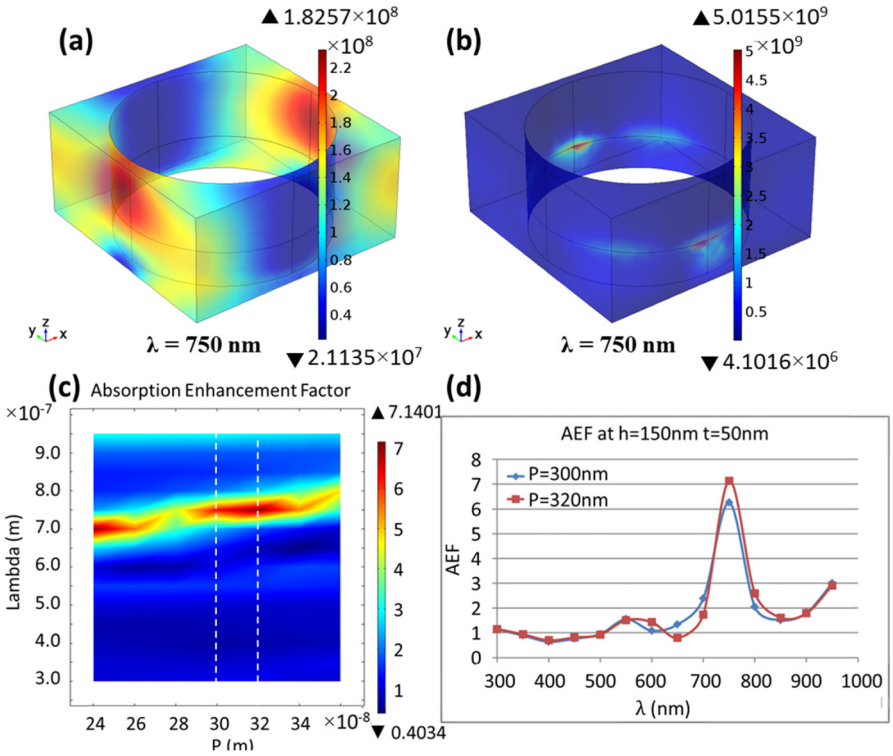

Fig. 3. E distribution at P = 320nm h = 150nm t = 50nm and λ = 750nm without (a) and with (b) gold filling. (c) mapping of absorption enhancement factor with respect to periodicity and incident wavelength and (d) re-plot of dash lines shown in (c).

Figure 4 reveals how coupling modes is related to periodicity and vertical dimension of holes for λ = 650 nm. At P = 300 nm (Fig. 4(a)), the electric field is less influenced by the

Optical Materials EXPRESS

variation of hole depth from 100 nm to 150 nm due to addition of gold. However, when P increases to 340 nm, the change in H leads to obvious change in E distribution (Fig. 4(b)): E couples mainly into TiO_2 domain for large H (H = 150 nm), but gets weaker and redistributes into the air domain as H decreases to 100 nm. At λ = 650 nm when P = 340 nm, the enhancement of electric field by SPR is not sufficient to compensate the decrease due to the recoupling in waveguide mode. Thus the total absorption in the corresponding region is reduced. For the same reason, the enhancement region is not continuous as observed earlier for thin film structures [10, 13].

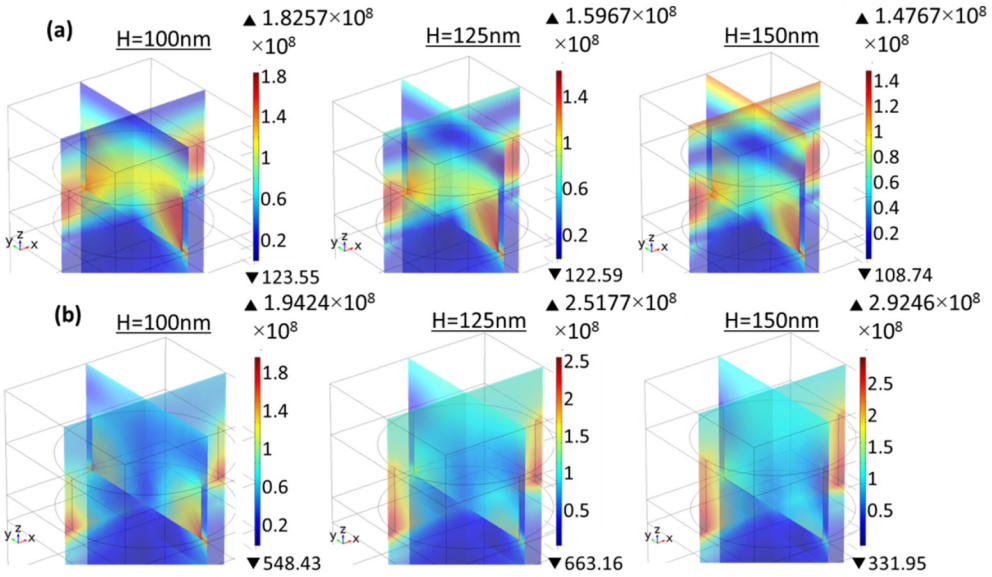

Fig. 4. E field distribution for different H and P at λ = 650 nm. (a) P = 300 nm, E couples both into the air and TiO_2 domains, and the strength of the field changes slightly; (b) P = 340 nm, E couples mainly into TiO_2 domain for longer hole structure (H = 150 nm), but gets weaker and redistributes into the air domain as h decreases to 100 nm.

Next, AEF mapping with t = 25 nm (Fig. 5(a), 5(b)) and t = 10 nm (Fig. 5(c), 5(d)) (other parameters remain the same) are analyzed. In both cases, absorption at around λ = 400 nm is improved. This is because, according to the aforementioned hypothesis, that reducing thickness of gold disks results in a lower aspect ratio (t: d), which consequently shifts the absorption spectrum of the gold disks out of visible region [28]. Since the absorption of gold is diminished, AEF of Au-TiO_2 system is correspondingly approaching unit. Another noticeable correlation is that when thickness of the gold disk is decreased to 25 nm or smaller, SPR effect still contributes to AEF but the resonance frequency is not affected by periodicity anylonger. As a matter of fact, dimensions of the metallic nanocrystals/nanoparticles used in most experimental work are 20 nm in [16] and 5 nm in [9, 15], all of which are smaller than 25 nm. This can partially explain why all the reports claim the same SPR region of λ ≈600 nm in spite of the synthesis and coupling methods of gold. However, as there exists no periodicity of nanoparticles formed by means of physical evaporation or chemical synthesis, more effort is required to put forward a more precise explanation to this phenomenon.

Optical Materials EXPRESS

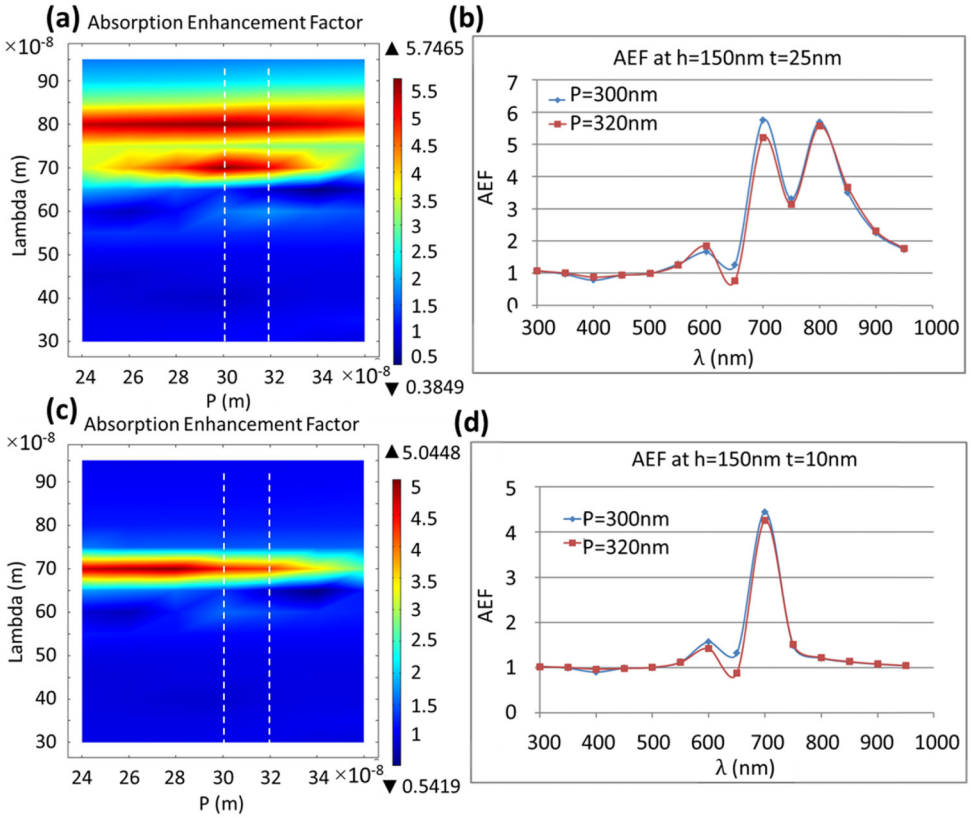

Fig. 5. Mapping of absorption enhancement factor with respect to periodicity and incident wavelength at (a) t = 25 nm (c) t = 10 nm. (b) and (d) plot the corresponding information following the white dashed lines in (a) and (c) respectively.

Compared to t = 50 nm and t = 10 nm, Fig. 5(a) (t = 25 nm) shows a much broader and continuous absorption band from 700 nm to 850 nm. Figure 5(b) has plotted AEF along the two white lines in Fig. 5(a), where two strong absorption peaks can be observed. The origin of these peaks can be found from Fig. 6. When λ = 700 nm (Fig. 6(a), 6(b)), both SPR effect indicated by white circles and coupling mode shown by black circles are visible on gold embedded TiO_2 nanohole arrays in Fig. 6(b). However, in the case of λ = 800 nm (Fig. 6(c), 6(d)), the coupling mode vanishes after inserting gold disks, leaving only SPR in Fig. 6(d) contributing to AEF. In addition, all three simulations show small peaks for incident wavelength from 550 nm to 600 nm, and their positions as well as the strength are varied by differing thickness of gold disks. Since these peaks are far below the SPR region, and can be affected by changing the depth (h) of the nanohole structures (results not shown here), they are most likely to be induced by cavity resonance.

Lastly, in order to find the relationship between depths of the nanohole structure (h) and its effect on absorption spectrum, a set of simulations were carried out by sweeping h from 150 nm to 1500 nm. Results revealed a clear SPR effect at the wavelengths between 700 - 800 nm. However, the SPR position does not change with h, meaning the SPR effect based on our proposed structure is insensitive to the depth of the initial nanohole structure. Based on this conclusion, we can expect very thin and light film for the electrode. To be more rigorous, all the simulations are also implemented under TM mode. The results (not shown) are as expected. Due to the symmetry in x and y dimension in the structure, every single simulation yields the same outcomes both qualitatively and quantitatively under TE and TM modes.

Optical Materials EXPRESS

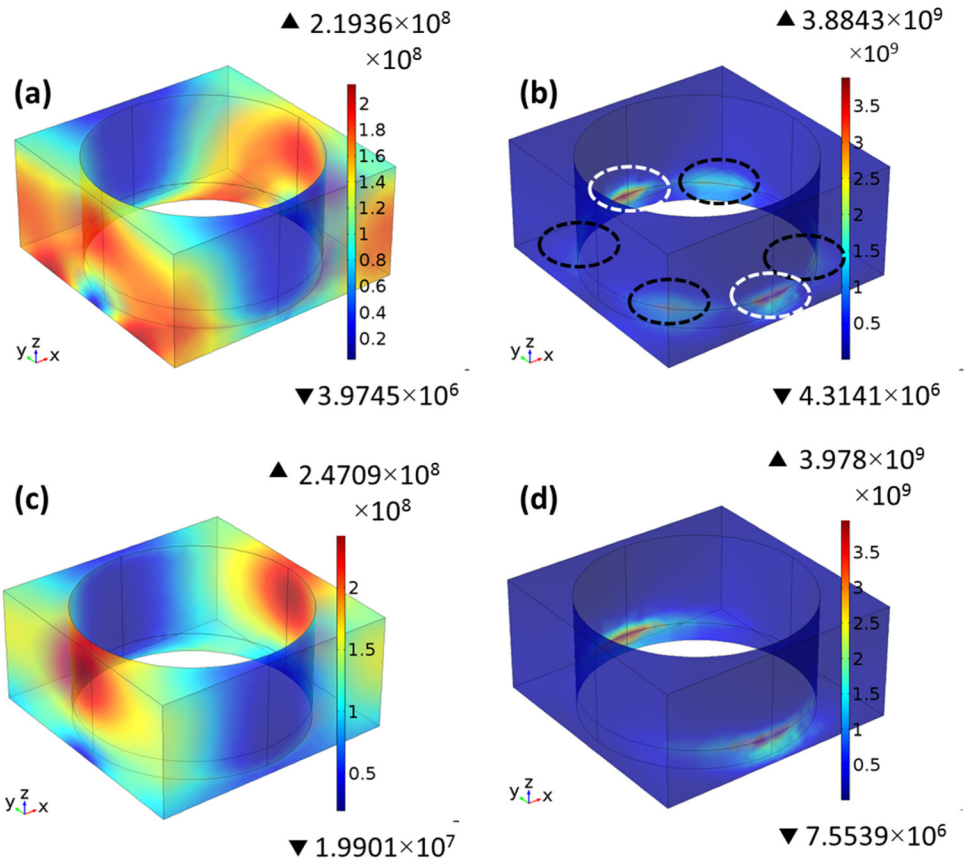

Fig. 6. Electric field distribution at λ = 700 nm (Fig. 6(a), 6(b)) and λ = 800 nm (Fig. 6(c), 6(d)) with (Fig. 6(b), 6(d)) and without (Fig. 6(a), 6(c)) gold disks. Comparing to the local fields from (a), the black circles in (b) indicate area where coupling mode is attributed to the absorption enhancement after adding gold to the holes, while the white circles stand for SPR effect. However, no obvious E enhancement can be found in (d) where coupling mode occurs in (c).

In addition to absorption enhancement under normal incidence, the reception angle of the proposed structure is also investigated. Incident angle (θ) from 0 to 45 degree are swept with other parameters being t = 25 nm, P = 320 nm and h = 150 nm. Figure 7(a) shows the AEF mapping with respect to incident wavelength and angle, and Fig. 7(b) is the re-plot of (a) but with maximum color range defined as 1. Taking a comparison between Fig. 7(a) and Fig. 5(a), we find that the maximum AEF value can reach 5 for most incident angles at resonance, *i.e.* 700 ≤ λ ≤ 850 nm. It is clearer in Fig. 7(b) that except for a limited region defined by θ ϵ (17, 34) deg and λ ϵ (450, 500) nm, the Au-TiO_2 system exhibits enhanced or similar absorption comparing to TiO_2 without gold in the entire mapping.

Optical Materials EXPRESS

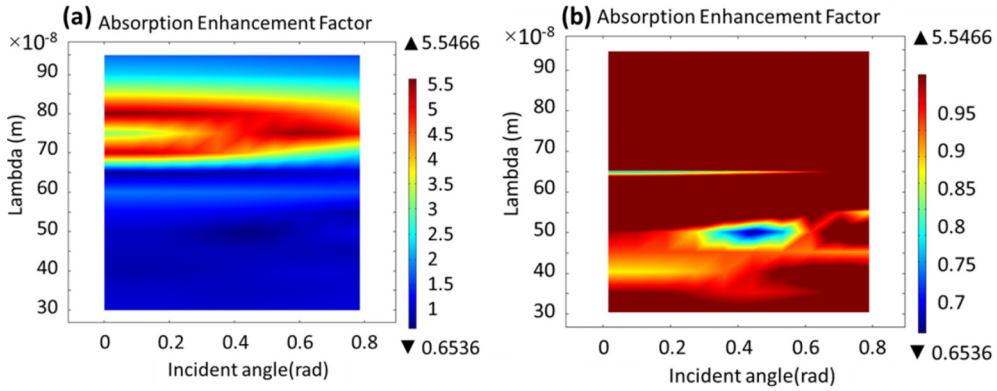

Fig. 7. Mapping of absorption enhancement factor with respect to incident angle and incident wavelength at t = 25 nm, P = 320 nm and h = 150 nm. (b) is a re-plot of (a) with maximum color range being unit.

4. Conclusion

A novel TiO_2 nanohole array structure embedded with gold disks is proposed for absorption enhancement of solar light. By using the TiO_2 nanohole arrays as template, plasmonic metal structure can be effectively patterned and possess a certain periodicity defined by the template. Additional gold fillings inside these nanohole arrays can improve absorption at a wide reception angle and promote a strong surface plasmonic effect at plasmonic frequency (λ = 700 - 850 nm for the selected periodicity and material described in this study) while still maintaining the same absorption in the low wavelength range. The absorption enhancement factor is calculated based on the nanohole array structure which originally has strong coupling to waveguide modes. As a result, only peaks induced by SPR effect are evident in the mapping graphics. The SPR frequency shifts along periodic orientation when thickness of the metallic layer exceeds 50 nm, which partially explained why small nanoparticles were reported to generate SPR at similar wavelength region despite of size and distribution. In addition, small peaks above the SPR frequency are observed from the plots which can be attributed to the cavity resonant. Due to the symmetric arrangement of the arrays, the proposed design gives the same behavior under both TE and TM modes. This model allows for precise control of shape and periodicity/distribution of the plasmonic metal nanodisks embedded into 1D semiconductor nanostructures. With such confined metallic structure, SPR can be better manipulated and contribute accordingly for different applications. The proposed model involves only conventional fabrication process and can be easily adapted to other solar active material combinations such as silicon/Ag system.

Funding

Norwegian Research Council-FRINATEK programme (231416/F20, 221860/F40); EEA-Poland (237761).

Acknowledgements

This work is supported by KD program at University College of Southeast Norway and Norwegian PhD Network on Nanotechnology for Microsystems, which is sponsored by the Research Council of Norway, Division for Science, under contract no. 221860/F40.